Polymer 187 (2020) 122101

Contents lists available at ScienceDirect

Polymer

journal homepage: http://www.elsevier.com/locate/polymer

Crystallization kinetics and morphology of small concentrations of cellulose nanofibrils (CNFs) and cellulose nanocrystals (CNCs) melt-compounded into poly(lactic acid) (PLA) with plasticizer

Caitlyn M. Clarkson [a], Sami M. El Awad Azrak [a], Gregory T. Schueneman [b], James F. Snyder [c], Jeffrey P. Youngblood [a,*]

[a] School of Materials Engineering, Purdue University, West Lafayette, IN, 47907, USA
[b] Forest Products Laboratory, Madison, WI, 53726, USA
[c] Army Research Laboratory, Adelphi, MD, 20783, USA

ARTICLE INFO

Keywords:
Poly(lactic acid)
Nucleation
Nanocellulose
Avrami kinetics
Crystallization

ABSTRACT

In the present study, very small concentrations of CNCs and CNFs were melt-compounded into PLA using a solvent-free process where poly(ethylene glycol) (PEG) was used to disperse the nanoparticles in PLA. As a comparison, the commercial nucleant, talc, was processed similarly into PLA. CNC and CNF were shown to be efficient nucleants for PLA, similar to talc, and conventional Avrami and Lauritzen-Hoffman analysis of the crystallization behavior was performed for isothermal temperatures from 90 °C to 130 °C across all compositions. From the Avrami analysis, the crystallization rate, half-time, and Avrami exponent were calculated and suggested a synergistic effect of nanocellulose and PEG, even at very small concentrations. The crystallization half-time was lower than talc at higher temperatures indicating faster crystallization for samples containing nanocellulose under certain conditions. Analysis of secondary nucleation revealed a decrease in the surface energy for CNC containing samples, further suggesting that, given the enhanced mobility of plasticized PLA, very small concentrations of CNC are effective nucleation agents. Lastly, scanning electron microscopy was used to correlate the crystal morphology of chemically etched samples with the thermal analysis. Coarsening of the microstructure was observed initially with the addition of PEG, and further coarsening was observed upon the addition of nanocellulose.

1. Introduction

Polylactic acid (PLA) has generated interest because it can be synthesized from corn, and is thus inherently more renewable than conventional, petroleum-based polymers [1,2]. In 3D printing, it is used for its ease of use and printability, i.e. its low melting point (150–170°) and desirable melt viscosity; e.g. PLA is being investigated as a material for 3D printed scaffolds [3]. While its other uses are predominately in packaging and consumer goods, there are drawbacks to using PLA in these applications [2,4]. The glass transition temperature (T_g) is between 50 and 60 °C, it has a low heat deflection temperature also around 50–60 •C and can be brittle [4]. Compared to other commercial consumer goods plastics, it is typically limited to short-term, single-use items that are used at room temperature, e.g. plastic utensils, cold-drink cups, and thermoformed lunch boxes-not reusable plasticware, plastic film, etc. [2,4]. Some of the properties of PLA could be improved by enhancing its crystallinity. However, PLA is a slow crystallizing polymer and without additives to increase the rate of crystallization, crystallinity in PLA is typically low after processing [2].

Nanocellulose, high-aspect ratio particles derived from wood, cotton, tunicates, bacteria, and various other sources, have inspired interest due to their remarkable properties and renewability [5–7]. Within the broad class of nanocelluloses are cellulose nanocrystals (CNCs) and cellulose nanofibrils (CNFs) [5]. CNCs are rod-like, highly crystalline (54–88%), nanoparticles with dimensions between 5 and 20 nm wide and 20–500 nm long that possess excellent stiffness (110–220 GPa) and strength (7.5–7.7 MPa) [5,6]. CNFs are nanoparticles with lengths up to 10 μm, typically higher amorphous content than CNCs, and which have shown good potential as a mechanical reinforcement in polymers due to high entanglement density [5]. Additionally, nanocellulose has

* Corresponding author.
E-mail address: jpyoungb@purdue.edu (J.P. Youngblood).

https://doi.org/10.1016/j.polymer.2019.122101
Received 18 October 2019; Received in revised form 12 December 2019; Accepted 18 December 2019
Available online 19 December 2019
0032-3861/

potential for enhanced thermal properties [8,9] and gas barrier behavior [10]. Hydroxyl groups present on the surfaces of both CNCs and CNFs govern dispersion and are a common site for surface modification to achieve dispersion in various media [6,11,12].

Plasticization and heterogeneous nucleation of PLA have been investigated to increase total crystallinity and accelerate the crystallization rate of PLA, which is relatively slow [2]. Typical plasticizers for PLA and PLA blends include citrate esters, glycerol, polyethylene glycol (PEG), and polypropylene glycol [13–15]. Although plasticizers can impart many benefits, there is a trade-off with performance. For instance, plasticizers increase ductility and toughness but typically decrease stiffness and strength. Nucleation agents and fillers can mitigate losses. Nucleation agents and fillers, which reduce the surface energy requirement for stable nuclei formation, impact the crystallinity by increasing the number of crystallites. Talc is a common nucleation agent/filler in PLA when faster crystallization kinetics are desirable [2,14,16]. The combination of plasticizers and nucleation agents has a synergistic effect on the crystallization rate. For instance, the addition of talc to PLA can reduce the crystallization half-time significantly, but the addition of PEG and talc further reduces the half-time and extends the crystallization window to lower temperatures [14].

Acquisition of more efficient and renewable nucleation agents has inspired exploration and development of various organic materials from nanocellulose, including pristine CNCs [17] and lignin-coated CNCs [18]. The efficacy of nanocellulose as a heterogeneous nucleation agent depends on specific surface area and dispersion in the polymer matrix. However, while nanocellulose has a high specific surface area to volume ratio which is good for nucleation, native CNC/CNF has poor compatibility with PLA and so disperses poorly leading to aggregation and inefficient crystallization. Commonly, organic solvent has been used to overcome this issue [17,19,20]. However, surface grafting has also been employed to improve the compatibility of nanocellulose with PLA through various modifications [21,22], utilizing grafted PLA chains [1,23], as well as grafting of known-plasticizers, like PEG, onto CNCs and CNFs [24,25]. However, using unmodified nanocellulose may offer significant cost savings if dispersion can be achieved. Some of the potential benefits of exploring organic nanoparticles as nucleation agents are speeding up crystallization kinetics or reducing crystallite size, as well as increased optical transparency, and tertiary effects like modifying the rheology of the polymer melt.

In many cases, the observed effects on crystallization are not intended as the CNC/CNF are used as reinforcements, and as such the concentration is high (above 1.0 wt%), while typical nucleant concentrations are much lower. Concentration is a critical parameter in promoting nucleation as above a critical concentration many heterogeneous nucleation aids, including nanocellulose, can inhibit molecular processes due to network formation. Gupta et al. demonstrated that lignin coated CNCs could be efficient nucleation aids at small concentrations (0.3%), but did not explore lower concentrations after observing that 0.1% of the lignin-coated CNC did not improve crystallization rates in PLA [18]. Moreover, CNC and CNF have been shown to affect the crystallization of PLA [18,20,24–27], but the majority explored high concentrations that bear little relevance to more typical nucleant concentrations.

The present work explores the combination of nanocellulose and plasticizer, specifically PEG, on the crystallization kinetics and morphology of PLA. To disperse nanocellulose in PLA, nanocellulose (CNC and CNF) were melt-compounded into PLA using a method reported by Clarkson et al. where CNC and CNF were first mixed with low molecular weight PEG through a process similar to conventional solvent exchange [22]. The solvent-free CNC/PEG and CNF/PEG solid solutions were melt-compounded into PLA to produce a fixed content of 5 wt% PEG and very small concentrations of CNC or CNF. Avrami analysis was performed on isothermal data spanning 90–130 °C and melting peak data was collected for all thermal histories for a Hoffman-Weeks estimate of the equilibrium melting temperature. Lastly, secondary nucleation theory was applied to further quantify the nucleation efficiency and the morphology was analyzed by scanning electron microscopy for select isothermal histories.

2. Materials & methods

Two types of nanocellulose were purchased from the University of Maine, Oronoa, ME, USA: Mechanically fibrillated CNF (Lot #U22; 3 wt % CNF-water slurry; 90% fines) and sulfuric acid-derived CNCs (2014-FPL-CNC-065; 11.9 wt% CNC-water slurry; 0.99 wt% sulfur on dry CNC) [5]. Transmission electron microscopy (TEM) images for these materials are provided in the supporting information, Fig. S1. CNC dimensions were 8.2 ± 7 nm by 91.7 ± 35.2 and CNF were 45.7 ± 18 nm wide and length dimensions exceeded the TEM view. Polyethylene glycol (PEG) was purchased from Millipore Sigma, St. Louis, MO, USA (Mn = 600 g/mol) and Nature Works INGEO-3001D poly(lactic acid) was purchased from Jamplast, Ellisville, MO, USA. The comparison material, Acros Organics talc (Lot A0381563; <75 μm/-200mesh; MW = 379.26 g/mol), was purchased from VWR International, Radnor, PA, USA. De-ionized, ultra-clean water was produced in house using a Barnstead device and was used for all solutions to avoid extra contamination.

As reported elsewhere, prior to compounding, solutions of CNC and CNF with PEG were prepared [22]. In brief, a solution of PEG in water was prepared by mechanically mixing. Meanwhile, CNC and CNF solutions were diluted with water and ultrasonicated using a Branson Ultrasonifyer at 30% power amplitude for 30 s with a 1 s pulse and 1 s rest for a total energy of 1800 J/g CNC. The respective CNC and CNF solutions were then poured into the PEG/water solution and allowed to mechanically mix on low heat for several hours prior to being ultrasonicated similarly a second time. A rotary evaporator at 70 °C and 125 Torr was used to remove the bulk of the water from the nanocellulose/PEG solution. A higher vacuum (2 Torr) at 70 °C was used to remove the remaining water. The procedure was used to create 1 wt% and 10 wt% CNC in PEG and 1 wt% CNF in PEG solutions; initial dispersion of nanocellulose in PEG is shown in polarized optical micrographs in the supporting information (Fig. S2). The 1 wt% CNC solution showed the best dispersion with little to no micron scale agglomerations, while increasing to 10 wt% CNC some agglomerations are present in the material (Fig. S2). The 1 wt% CNF shows evidence of agglomerations and entanglements which is expected since, as Fig. S1 shows, CNF entanglements can persist despite best efforts to disperse the nanoparticles (Fig. S2). Using this method, it was difficult to obtain higher concentrations of CNF in PEG for comparison to the CNC nanocomposites as the CNF starts at a much lower concentration in water compared to CNC and phase separation was a concern. Immediately after drying, the CNC/PEG and CNF/PEG solutions were injected with a syringe-style hopper into PLA (dried at 100 °C for 12hrs) at fixed quantities to produce the following compositions with 5 wt% PEG: 0.05 wt% CNF, 0.05 wt% CNC, and 0.55 wt% CNC. Talc was premixed with PEG to produce a 1 wt% solution for compounding using mechanical mixing and ultrasonication in line with the method used to prepare the nanocellulose compositions. Compounding was performed in a twin-screw 5 cc Xplore micro-compounder with continuous feed hopper at 200 °C and 100 rpm for 5 min for all compositions. Cross-polarized optical microscopy of all samples showing dispersion is in Fig. S3 of the supporting information.

All thermal experiments were performed in a Thermal Analysis (TA) Q800 differential scanning calorimeter (DSC). Samples were prepared in hermetically sealed aluminum pans with a mass of 11.1 ± 2.9 mg. For non-isothermal experiments, materials were first held at 200 °C for 2–5 min, quenched at 50 °C/min and reheated to 200 °C at 10 °C/min; experiments were run in triplicate Isothermal experiments were performed by first allowing the materials to fully melt at 200 °C for 3–5 min then quenching (50 °C/min) to the desired isothermal temperature (T_c = 90 °C, 100 °C, 115 °C, 120 °C, and 130 °C). All samples were held until crystallization had completed (indicated by a flat baseline) prior to a

quench to 0 °C and subsequent heat at 10 °C/min to 200 °C.

An FEI Quanta 650 FEG scanning electron microscope (SEM) was used to image crystal morphology for chemically etched specimens. For this analysis, DSC samples were removed from the aluminum hermetic pans after isothermal aging at 90 °C or 130 °C and then quenched to room temperature. Chemical etching of isothermal specimens was performed by submersing specimens in a solution of 0.025 mol/L NaOH in a 1:1 ratio of water/methanol for 4 h at 65 °C following the procedure of He et al. [29,30]. After etching, samples were rinsed with water and methanol, then dried in high vacuum for 30 min at room temperature to remove any residual solvent. Samples were sputter-coated prior to imaging with palladium/gold using an SPI Sputter Coater. SEM parameters for imaging were as follows: small working distance of 9–12 mm, 2–5 KeV accelerating voltage, and a spot size of 3–4.

3. Results and discussion

3.1. Avrami crystallization kinetics

Non-isothermal and isothermal history data capture the complex relationships of nucleation and growth with time and temperature and the effects of these different thermal histories can be observed in subsequent heating cycles. The following parameters were measured from DSC thermograms: glass transition (T_g) measured as the inflection point, cold crystallization temperature (T_{cc}) taken as the peak temperature, and melting point $T_{m\ 1\ or\ 2}$ as the temperature at the minimum of the well. T_{m1} is the melting point of the first melting peak (if exhibited) and T_{m2} is the second melting peak. The appearance of two melting peaks in PLA is commonly associated with the formation of the ordered and disordered α and α' phase, respectively [31–33]. The enthalpy of melting, ΔH_m and enthalpy of cold crystallization, ΔH_{cc}, are opposite in sign and were used to calculate the relative degree of crystallinity, χ, from equation (1) where ΔH_m° is the theoretical maximum melting enthalpy, 93 J/g [21,27,28,34]. For samples exhibiting an exothermic shoulder immediately before melting, the area under this peak was also subtracted from ΔH_m; details are published in the supporting information (Fig. S4).

$$\chi(\%) = 100\% \frac{(\Delta H_m + \Delta H_{cc})}{\Delta H_m^o (1 - w_{NC} - w_{PEG})} \quad (1)$$

A quench and subsequent heat indicated no detectable crystallization upon cooling at 50 °C/min for the compositions explored and provided a baseline for material properties (Fig. 1). The materials properties (T_g, T_{cc}, and T_{m1}, T_{m2}) measured upon heating from Fig. 1, were recorded in Table 1. Compared to the neat PLA, all compositions showed a decrease in T_g, T_{m1} and T_{m2}, although only neat PLA and 0.05 wt% talc exhibited strong double melting peaks (Fig. 1). T_g suppression is one of the measures for determining plasticizer efficiency and the observed values are comparable in magnitude to other PLA/PEG studies [34,35]. Likewise, decreased T_{cc} and T_m have been observed with the addition of nanocellulose as well as talc, which agreed with previous crystallization studies for both classes of materials [14,18,36]. Importantly, a decrease in T_{cc} (Table 1) can be desirable as it implies that the crystallization window is moving to lower temperatures. For processing, this is better as thermal gradients in the part govern the degree of crystallinity throughout the component and by expanding this window, the crystallinity for the entire component can effectively be increased or the processing temperature can be lowered leading to more efficient processes.

The crystallization window provided by the temperature range of T_{cc} was the basis for selection of isothermal crystallization temperatures, T_c, and isothermal experiments were run at 90 °C, 100 °C, 110 °C, 115 °C, 120 °C, and 130 °C. While growth is favored at higher T_c, investigation of low T_c is industrially relevant as many plastic components are exposed to cooler surfaces during processing. For instance, low mold temperatures in injection molding are desirable as reducing mold temperature

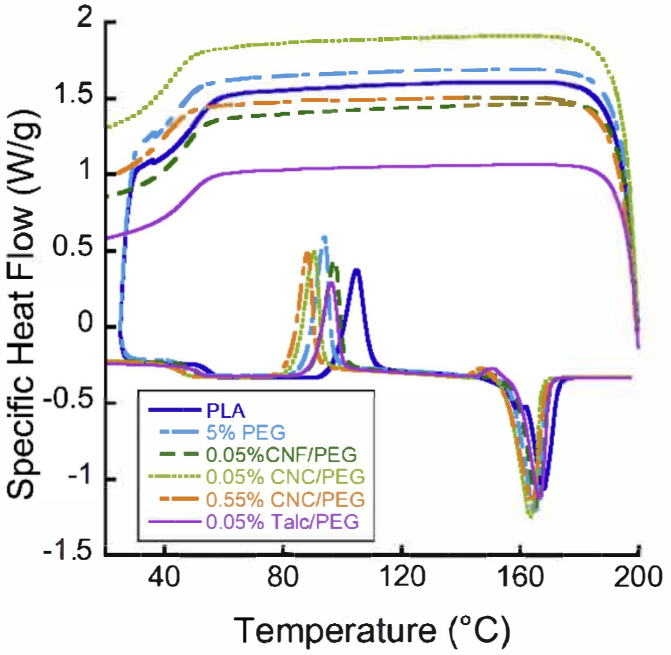

Fig. 1. Experimental data for a 50 °C/min cool followed by subsequent heating at 10 °C/min.

Table 1
Thermal properties measured from non-isothermal experiments.

Sample	Nanocellulose (wt%)	PEG (wt %)	T_g(°C)	T_{cc}(°C)	T_{m1}(°C)	T_{m2} (°C)
Neat PLA	0	0	58.6 ± 2.7	105.3 ± 1.0	161.3 ± 1.6	168.4 ± 1.0
PEG	0	5	48.2 ± 0.1	92.3 ± 1.0	–	164.1 ± 0.2
CNF/ PEG	0.05	5	48.4 ± 1.8	94.4 ± 2.0	–	165.2 ± 0.5
CNC/ PEG	0.05	5	44.9 ± 1.0	88.0 ± 2.0	–	163.4 ± 0.4
	0.55	5	45.8 ± 1.0	88.6 ± 1.2	–	163.6 ± 0.2
Talc/ PEG	0.05	5	50.4 ± 3.2	95.7 ± 4.2	–	164.7 ± 1.8

reduces cycle times and lowers cost if the mold does not have to be heated as high in temperature. As an example, in Fig. 2A–C, specific heat flow, $\Delta H(t)/\Delta H_{total}$, which has been used to calculate relative crystallinity conversion, χ_c, is shown for 100 °C. Generally, a steep slope suggests faster crystallization kinetics. From 100 °C to 130 °C, χ_c is observed to take longer and longer times to complete conversion ($\chi_c = 1$) for a specific T_c. At the lowest T_c, 90 °C, χ_c is observed to shift right as well, suggesting that the maximum crystallization rate is between 90 and 110 °C. To quantitatively determine the crystallization rate, the Avrami formalism was employed.

Analysis of the isotherms was performed in Origin® with a custom Origin® plugin designed for Avrami and Lauritzen-Hoffman analysis by Lorenzo et al. [37]. In brief, a baseline was subtracted from the isotherms, for example, Fig. 2A and converted to χ_c shown in Fig. 2B (all temperatures in Fig. S5 and Fig. S6 in supporting information). The mass fraction of crystallized material, w_c, shown in Eq. (2) is proportional to χ_c. The volume fraction of converted material (V_c) is then calculated from Eq. (3), where the amorphous and crystalline densities were assumed to be $\rho_a = 1.25$ g/cc and $\rho_c = 1.359$ g/cc for poly(L-lactic acid) (PLLA). The software uses equations (2)–(5) to create the 'Avrami plot'

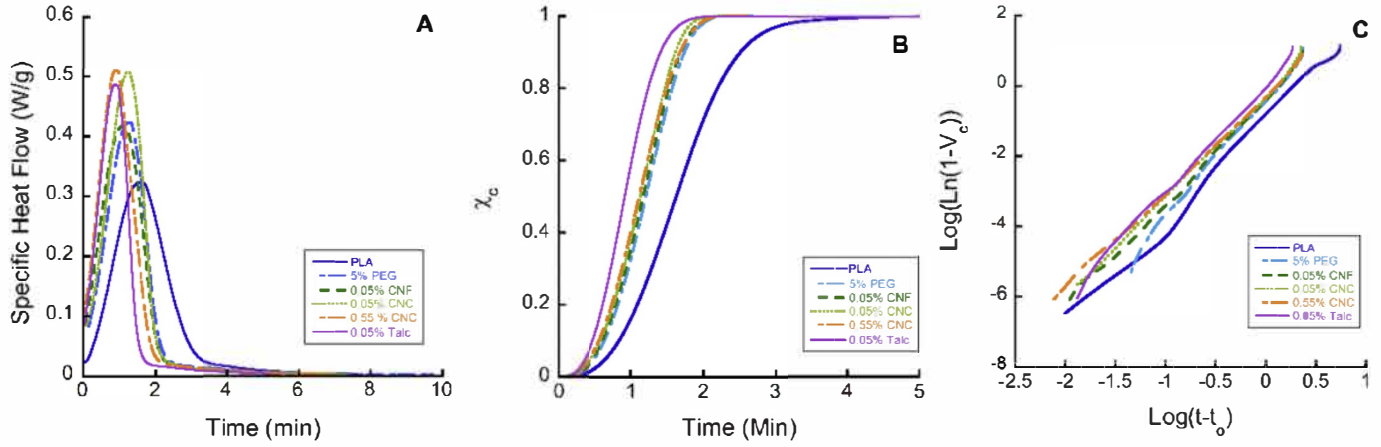

Fig. 2. Progression of Avrami analysis from isothermal data at 100 °C: A) Experimental isothermal data, B) Crystallinity conversion versus experiment time and C) Avrami type plot of Log(Ln(1-V_c)) vs Log(t-t_o).

of Log(-Ln(1-V_c)) vs. Log(t-t_0). A representative plot is shown in Fig. 2C. The Avrami index (n) and rate constant, k, were determined from a linear regression of the Avrami plot for V_c = 1–40% to obtain an R^2 = 0.99. The rate constant, k combines the nucleation and growth rate contributions to describe the total crystallization rate. The Avrami exponent, n, is a value between 1 and 4 and is the sum of the dimensionality, n_d, and nucleation, n_n, components [38]. Theoretically, n_d can be integer values of 1, 2, or 3, and n_n can be either 0 (instantaneous nucleation) or 1 (sporadic nucleation) [38]. However, non-integer values of n are often observed because many materials are thought to be in a transition state between clearly defined modes. Generally, the morphology of the sample corresponds with $n = 1$ for a line, $n = 2$ is a sheet, and above $n = 3$ are spherulites [38]. Lastly, time for 50% conversion or the half-time, $\tau_{1/2}$, can be calculated from Eq. (6) [18,29,39]. These values are recorded in Table 2.

$$w_C \tilde{\chi}_c = \frac{\Delta H(t)}{\Delta H_{total}} \tag{2}$$

$$V_c = \frac{W_c}{W_c + \left(\rho_c/\rho_a\right)(1 - W_c)} \tag{3}$$

$$1 - V_c(t) = \exp(-kt^n) \tag{4}$$

$$\mathrm{Log}[-\mathrm{Ln}[1 - V_c(t)]] = \mathrm{Log}(k) + n\mathrm{Log}(t) \tag{5}$$

$$\tau_{1/2} = \left(\ln(2)/k\right)^{1/n} \tag{6}$$

As the growth rate depends on the diffusion of polymer chains, the addition of PEG, which will improve molecular mobility, will affect the crystallization rate. Previous studies have observed improvement in crystallization for low molecular weight PEGs in PLA at concentrations of 5–20 wt% [35,40–42]. While it was expected that the addition of PEG would have a similar effect here, the effects were relatively small. In Table 2 and Fig. 3A, k was observed to increase slightly compared to the neat PLA, and $\tau_{1/2}$ decreased for T_c = 90–120 °C. The Avrami exponent, n, did not change significantly from that of neat PLA which was around $n = 3$ for 3 dimensional or spherulitic growth.

With the addition of nucleation agents, larger changes in k and $\tau_{1/2}$ were observed. The addition of CNC or CNF with 5% PEG caused k to increase more substantially than 5% PEG suggesting that CNC and CNF are improving crystallization rate, specifically at low T_c like 90 °C or 100 °C (Table 2, Fig. 3A). Consequently, an overall decrease in $\tau_{1/2}$ was also observed (Table 2, Fig. 3B). At 0.05% CNF and both CNC compositions, k more than doubled at T_c = 100 °C where the fastest

Table 2
Avrami isothermal kinetics data.

	Nanocellulose (wt%)	PEG (wt%)	T_c(°C)	$k(min^{-1})^n$	n	$\tau_{1/2}$(min)
Neat PLA	0	0	90	0.0312	3.1	2.73
			100	0.161	2.9	1.66
			110	0.06	3.0	2.27
			115	0.0086	3.1	4.26
			120	0.00091	3.1	8.78
			130	0.000012	3.6	21.1
PEG	0	5	90	0.096	2.7	2.06
			100	0.17	2.9	1.63
			110	0.072	2.9	2.18
			115	0.053	2.7	2.55
			120	0.0065	3.1	4.58
			130	0.0000528	3.1	21.9
CNF/ PEG	0.05	5	90	0.412	2.8	1.21
			100	0.404	2.9	1.20
			110	0.087	2.7	2.12
			115	0.027	3.0	3.04
			120	0.009	2.8	4.64
			130	0.00012	3.1	16.42
CNC/ PEG	0.05	5	90	0.435	2.6	1.17
			100	0.436	2.7	1.16
			110	0.166	2.7	1.67
			115	0.095	2.7	2.04
			120	0.055	2.8	2.47
			130	0.00026	3.0	14.26
	0.55	5	90	0.37	2.8	1.25
			100	0.47	2.7	1.14
			110	0.078	2.8	2.14
			115	0.039	2.8	2.78
			120	0.0099	2.9	4.20
			130	0.000179	2.9	18.21
Talc/ PEG	0.05	5	90	0.70	2.8	0.99
			100	0.84	2.8	0.93
			110	0.26	3.3	1.36
			115	0.186	3.0	1.53
			120	0.00265	3.9	4.3
			130	0.0000389	3.4	17.80

crystallization rates were observed for all conditions. While the talc composition was faster at low T_c, the CNC was faster at 120 °C and 130 °C and the CNF was faster at 130 °C. The comparison material, in this case, was a known nucleation agent for PLA, talc, and as expected, it improved the crystallization kinetics of PLA of which surface area and surface energy are important factors in determining nucleation efficiency [14]. Compared to CNC, the surface area/volume ratio of talc should be smaller since the talc particles were micron-scale, however, the surface energy of talc is probably lower than that of CNC or CNF at low temperature (Table S1 in supporting information). Furthermore, the

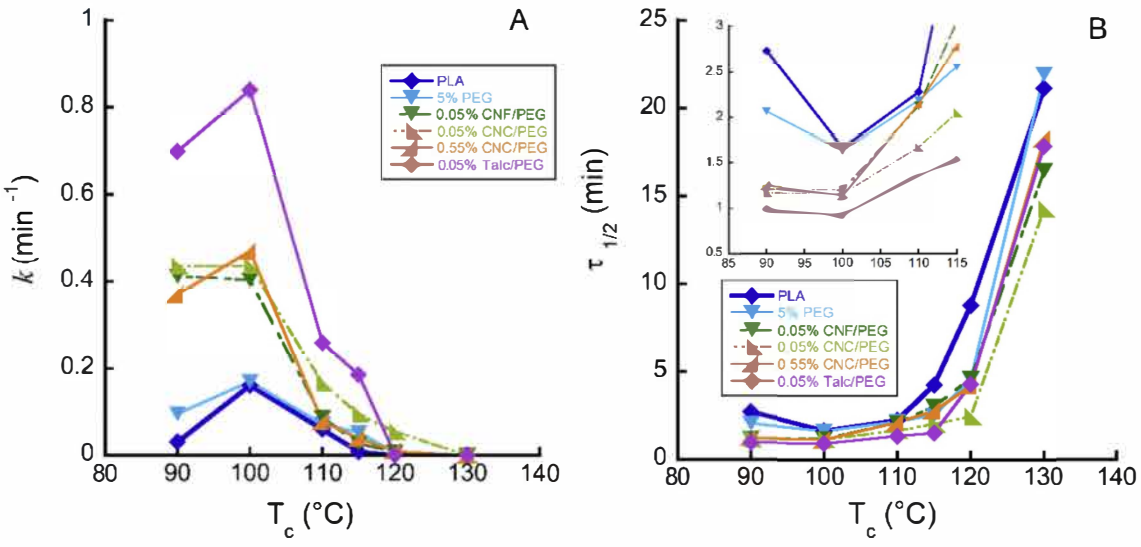

Fig. 3. A) crystallization rate, k, and B) Half-time, $\tau_{1/2}$, versus T_c for all compositions.

surface energy is not expected to remain constant with temperature. As Khoshkava and Kamal demonstrated, the surface energy of CNC at room temperature is above PLA, but at 190 °C, it is significantly lower [43]. This may explain why the CNC and CNF demonstrated faster crystallization at higher temperatures.

Interestingly, at low concentration, the crystallization rate of CNC and CNF are very similar despite the large difference in size between nanoparticles. Although CNFs have comparable widths, they are very long (several microns) compared to CNCs which are 5–20 nm wide and 20–500 nm long [5]. CNCs, which provide a higher total surface area per volume compared to CNFs are expected to be the superior nucleation agent. Also, CNFs have been observed to exhibit entanglements (Figs. S1 and S2) which further limit the available surfaces for nucleation as these entanglements will most likely be carried over into the composite to some extent.

Several potential reasons exist for the observation that the CNC and CNF effects at small concentration are very similar. First, surface energy differences between CNC and CNF may arise from the processing of these materials. The CNC has a sulfate half-ester that is substituted for some of the OH- in the acid hydrolysis process, which puts a negatively charged sulfate half ester, $-OSO_3^- H^+$, on the surface [44,45]. While the negative charge is effective at stabilizing CNC/water suspensions, it may also account for a slight change in surface energy making the CNC more hydrophilic compared to mechanically fibrillated CNF, and thus, less compatible with PLA. Comparing surface energy measurements for similar nanocellulose materials, this appears to be the case (Table S1). Secondly, the interfacial energy between the nanocellulose and PLA may be changed by the addition of a plasticizer such as PEG due to adsorption of the PEG onto the surface of CNC/CNF. A study by Angles et al. demonstrated that the interfacial energy between glycerol and cellulose whiskers was higher than the starch matrix these materials were meant to modify [46]. Thirdly, CNC/CNF may have a higher affinity for PEG than PLA causing partitioning of the PEG to the nanocellulose interphase. This has been observed for CNCs in polyurethanes where the CNC preferentially located in the polyol-rich soft blocks [47]. One would expect that a more hydrophilic CNC to be more affected than CNF. These additional factors could explain why the surface area is not the only driving factor in improving the crystallization rate.

While the nanocomposites showed no optical indication of agglomeration, sub-micron agglomerations could persist despite best efforts to distribute and disperse the nanoparticles. In turn, this could reduce the effective surface area. Numerous studies have investigated the use of PEG as a material to help re-disperse dried CNC and have shown that in *dried products*, PEG does shield neighboring CNC interactions and CNC/PEG exhibited reversible hydrogen bonding when re-dispersed in water [48]. They also showed that the shielding was not 100% effective as after redispersion particle size was still larger than before [48]. Though similar behavior may be expected in the dry nanocellulose/PEG solutions employed in the present study, between the two concentrations examined here, the degree of agglomeration in the 10 wt% CNC/PEG solution (Fig. S2), appears to be slightly higher than lower CNC counterparts. CNC agglomeration would result in a lower effective surface area/volume ratio despite more CNCs being present. This may explain why a significant improvement in rate or half-time was not observed between 0.05 wt% and 0.55 wt% CNC despite an over ten-fold increase in nanoparticle concentration. Alternatively, higher concentrations of CNCs acting as a barrier to molecular motion, such as growing crystallites, has been proposed in other materials and could be the case here as well, though the concentrations are much lower than expected [19].

3.2. Effects on melting behavior

Composition was shown to affect the melting behavior of isothermally crystallized samples as shown in Fig. 4. PLA commonly crystallizes into an ordered α phase and disordered α′ phase [31,49]. The two crystal structures are very similar and can be difficult to distinguish by wide-angle x-ray diffraction, however, the appearance of double melting peaks can be quite indicative of crystallization processes [31]. In poly (L-lactic acid) (PLLA), the α′ phase is known to crystallize at low T_c while α phase crystallizes at high T_c; the transition coincides with the appearance of the double melting peaks and the shoulder on the melting exotherm which sometimes appears is the α′ to α transition [31–33,50]. The α' phase is thought to undergo a solid-solid phase transition to the ordered α phase when an exothermic shoulder is observed during heating cycles [33]. Both phenomena were observed in Fig. 4. At 90 °C, PLA and 5 wt% PEG compositions exhibited distinct exothermic shoulders immediately before the melting endotherm. The samples containing nucleation agents exhibited a very shallow melting endotherm, except for 0.05 wt% CNC which exhibited a strong endotherm, instead. However, all samples exhibited the shoulder in the non-isothermal history which would have undergone crystallization over a wide temperature range (Fig. 1). After the materials switched to the melt recrystallization mechanism, either T_c = 90 °C or 100 °C, the peaks in Fig. 4 showed a distinct temperature dependence, where at low T_c the first melting peak is distinct from the second peak and as T_c increases, the two peaks become merged. At very high T_c, a single peak is observed (130 °C)

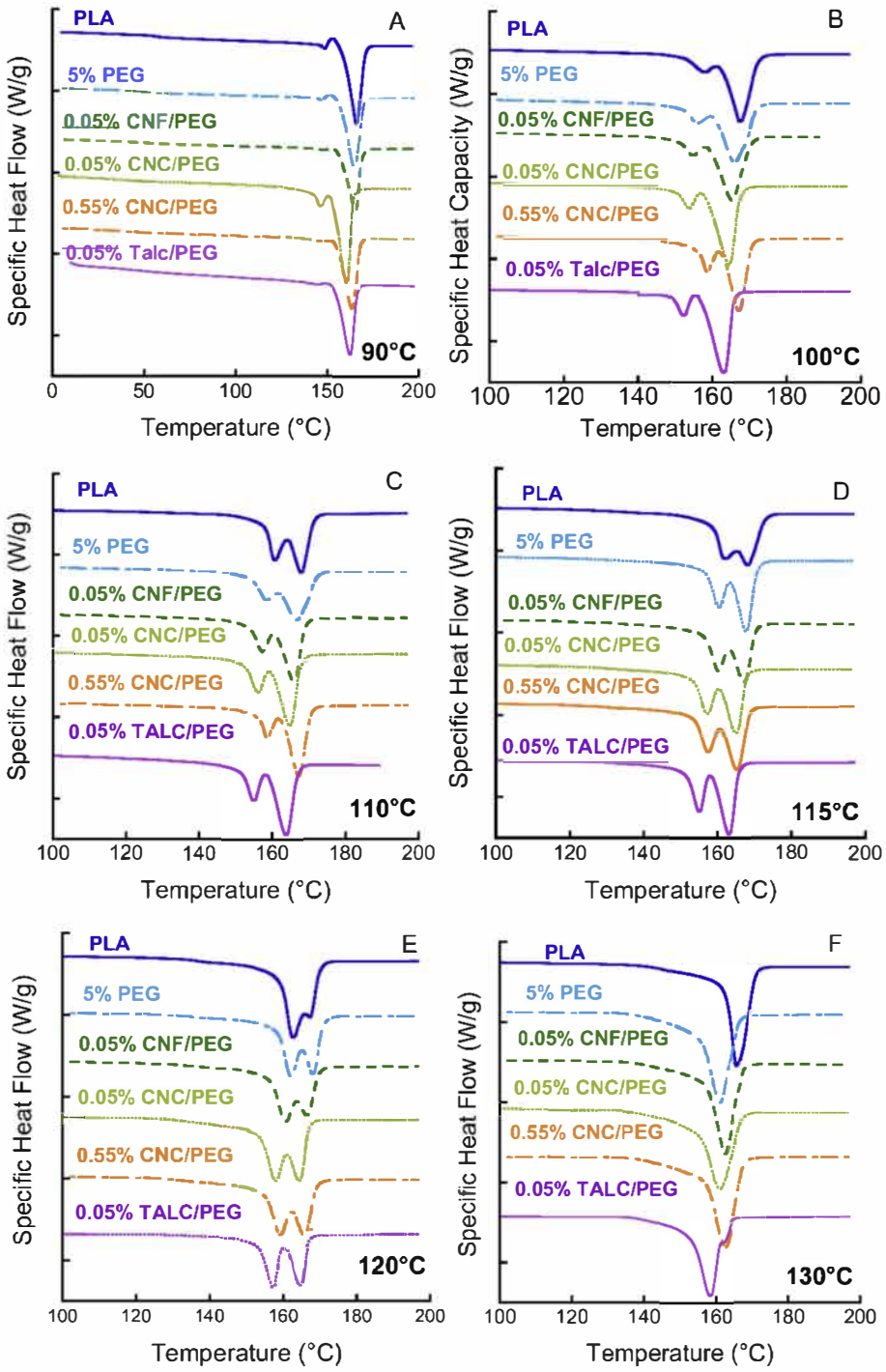

Fig. 4. Thermograms after isothermal crystallization at A) 90 °C B) 100 °C C) 110 °C D) 115 °C E) 120 °C F) 130 °C.

which agrees well with expectation [1,31]. While the melting points of peak 1, T_{m1}, increased with increasing T_c, T_{m2} showed only weak temperature dependence which is to be expected as at elevated temperature, reorganized/regrown crystals will be more uniform in size and perfection (Fig. S8 and Table S2 in supporting information). Of the nucleated compositions, talc exhibited the largest suppression in melting point, T_{m1}, followed by 0.05 wt% CNC, 0.55 wt% CNC, 0.05 wt% CNF, and then 5 wt% PEG (Fig. 5A; Table S2 in supporting information). Smaller T_{m1} and broadening of the melting endotherm, like in Fig. 4F, suggests a smaller and/or less perfect, but wider distribution of crystallite sizes. Since the k increased, it is expected that crystallite size, and therefore T_{m1}, should decrease because of more nuclei growing means a smaller average size before growing into a neighboring crystal. Melting point suppression suggested that the 0.05% CNC and 0.05% talc would be the fastest crystallizing materials since these materials would be expected to have the smallest crystallite size distribution. Slight variations in experimental melting points could be due to variation between samples as well as lamellar thickening during the thermal experiment either during crystallization or during subsequent heating. Regardless, a larger melting temperature can lead to higher temperature usage in polymers.

During isothermal crystallization, samples are held at T_c until the crystallization process is complete, and from the second heat, the degree of crystallinity, χ, can be calculated using equation (1). At higher T_c, the molecular mobility is higher and larger molecular weight chains can be

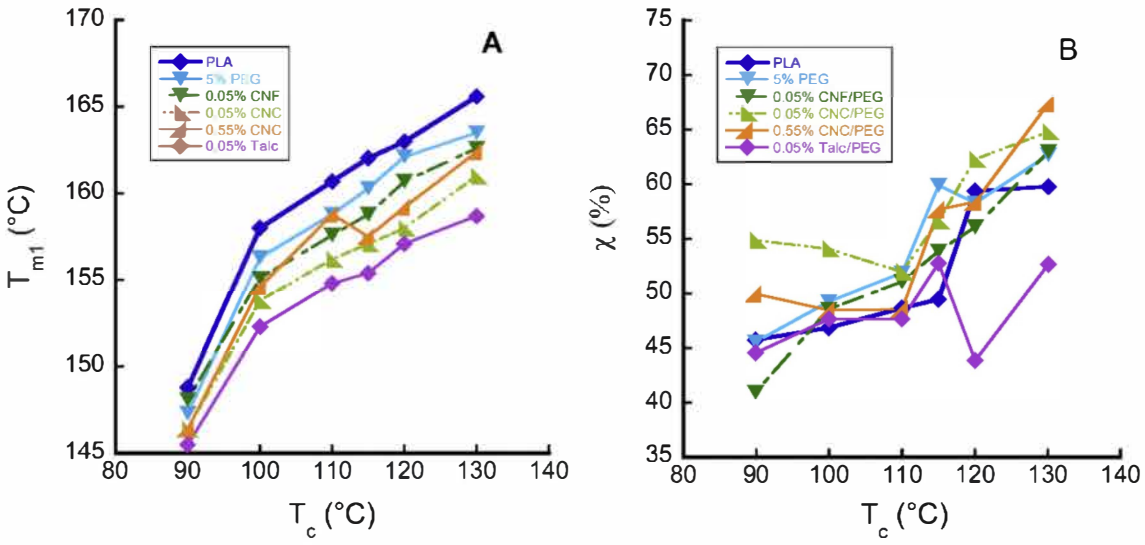

Fig. 5. A) T_{m1} versus T_c and B) the crystallinity, χ, versus T_c.

more easily incorporated into the crystal. Consequently, χ is observed to increase with increasing T_c over the range selected (Fig. 5B; Table S2 in supporting information). Although the total degree of crystallinity is improved at higher T_c, the rate of crystallization, Table 2, decreases with increasing T_c even if growth is favored at higher temperatures, and the time to complete crystallization at a given temperature dramatically increases. This is because, at higher T_c, nucleation is the limiting factor in determining the crystallization rate. Samples containing nanocellulose exhibited higher χ compared to the neat PLA, 5%PEG, and 0.05% talc. Interestingly, from Table 2, the half-time was comparable or smaller for these materials which suggests that the nanocellulose/PEG combination is improving growth in addition to nucleation, the primary contribution in improving the crystallization kinetics of PLA. Larger χ is generally correlated to better properties such as heat deflection temperature and gas barrier and is a major reason that nucleants are added to polymers. In this case, nanocellulose may be superior in some instances as it leads to higher overall crystallinity than nucleants such as talc.

3.3. Nucleation efficiency from secondary nucleation theory

Secondary nucleation theory provides access to additional information about nucleation efficacy and growth. Lauritzen and Hoffman's expression for the growth rate in Eq (7) consists of two primary components: the activation energy barrier for diffusion of chains to the growth front and the surface energy component to overcome during the addition of strands on a layer, i.e. the initial process of nucleation [38]. While the former is represented by the first exponent, the latter is represented in the second in which K_g is the nucleation constant. The growth rate data were approximated as, $G = 1/\tau_{1/2}$, and fit with equation (7), where $U^* = 1500$ cal/mol, $T_\infty = T_g$-30 °C (Table 1), R is the ideal gas constant, $\Delta T = T_m^\circ - T_c$, and f is a correction factor ($f = 2T_c/(T_c + T_m^\circ)$) [18]. The equilibrium melting temperature, T_m°, was estimated from a nonlinear Hoffman-Weeks extrapolation (Fig. S7 in supporting information) and is reported in Table 3 [38]. T_m° estimates were in the acceptable range for various PLA materials [18,29,50–54]. Variation in T_m° could be the consequence of lamellar thickening during the isothermal experiments [29]. Equation (7) was re-arranged and plotted in Fig. 6 where the slope of the line is K_g.

$$G = G_o exp\left(\frac{-U^*}{R(T_c - T_\infty)}\right)\exp\left(\frac{-K_g}{T_c \Delta T f}\right) \quad (7)$$

Surface energy terms which describe nucleation are buried in K_g (Equation (8)). In equation (8), K_g is the energy required for nuclei of a critical size to form which depends on several factors such as the free energy of folding, σ_e, the lateral surface energy, σ, thickness of a single layer, b, the Boltzmann constant, k_B, enthalpy of melting per unit volume, ΔH_f, and n, which corresponds to the three crystallization regimes [38]. The three regimes are: regime I, regime II, and regime III [38]. In regime I and regime III, $n = 4$ and in regime II $n = 2$ [38]. Polymers can exhibit a combination of the regimes or a single regime. PLA most often exhibits regimes II and III [51,55].

Table 3
Parameters from secondary nucleation theory.

Material	T_m° (°C)	K_g (10^5 K^2)	σ_e (erg/cm^2)	σ (erg/cm^2)	$\sigma\,\sigma_e$
NeatPLA	207.4	8.69	217.3	7.02	1525.5
5 wt% PEG	202.8	6.71	169.3	7.02	1188.5
0.05 wt% CNF 5 wt% PEG	202.4	6.97	176.1	7.02	1236.2
0.05 wt% CNC 5 wt % PEG	196.2	5.51	141.0	7.02	989.8
0.55 wt% CNC 5 wt % PEG	199.0	5.7	146.1	7.02	1025.6
0.05 wt% Talc 5 wt% PEG	188.8	5.0	130.2	7.02	914.0

$$K_g = \frac{nb\sigma\sigma_e T_m^o}{\Delta H_f k_B} \quad (8)$$

All compositions exhibited linear behavior in Fig. 6 After testing multiple possible regimes for $KgIII/KII = 2$ by measuring the ratio of slopes between high and low T_c from Fig. 6, there was no conclusive evidence that any of the compositions exhibited a second regime above 115 °C. The slopes in Fig. 6 are observed to decrease as the composition is changed which indicated that the energy for nuclei to form is decreasing as well. Theoretically, T_m° should not change since only the PLA is crystallizing. However, for the present study, unique T_m° were estimated for each composition and so, the data is also observed to shift right as the experimentally fit T_m° was observed to decrease for the more efficient nucleating compositions. The exhibited regime was assumed to be regime III as regime 3 is the commonly observed regime in PLA and is typically reported to cover the temperature region below 115–125 °C. The parameters used for the custom Origin plugin developed by Lorenzo et al. where: a = 5.17, b = 5.97, and $\Delta H_f = 1.26 \times 10^8$ J/m^3 [37]. The results of the linear regression of Fig. 6 are shown in Table 3 where the slopes of the trend lines, K_g, are tabulated and additional parameters

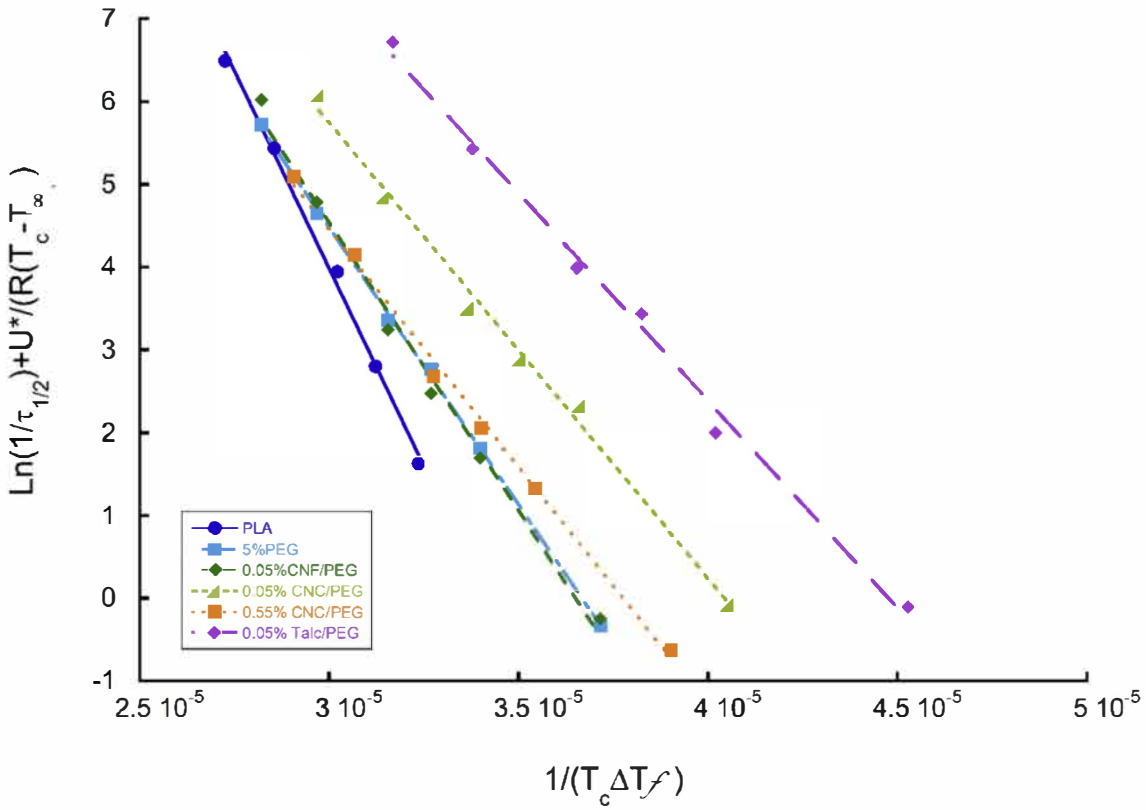

Fig. 6. Plot of $\mathrm{Ln}(1/\tau_{1/2})+U^*/(R(T_c-T_\infty))$ vs. $1/(T_c\Delta Tf)$.

from Eq. (8) have been calculated and reported.

From Table 3, it was observed the K_g and σ_e both decreased with the addition of PEG and nucleation agents. From Table 3, σ_e was observed to decrease for all compositions. The reduction in σ_e was largest for talc, followed by CNC indicating that, at this concentration, these materials are the superior nucleation agent as the energy requirement to create a new fold is reduced in the presence of a desirable nucleation surface. Between 0.05 wt% CNC and 0.55 wt% CNC, σ_e was very similar (141 and 146.1 erg/cm^2) which is to be expected and the difference between the two concentrations is acceptable in light of previous CNC concentration studies [18]. At small concentrations, CNCs are not expected to form a percolation network which can inhibit crystallization and the difference in σ_e may simply be due to variation in fitting of the growth rate or T_m or experimental variation. The 5 wt% PEG and 0.05 wt% CNF appear to be very similar in Fig. 6. Addition of PEG produced a decrease in K_g indicating that increasing the mobility of PLA chains is enough to reduce σ_e while addition of 0.05% CNF did not further reduce σ_e or K_g.

3.4. Crystal morphology

Crystal morphology is of key interest as crystallite size and morphology, in part, determine materials properties such as opacity or melting point. Neat PLA and PLA blends have been previously shown to exhibit banded spherulitic structures under certain conditions [56–58]; e.g. blends of poly(ethylene oxide) (PEO) and PLA exhibited highly periodic banded spherulites when crystallized at 125 °C [56]. The morphology of compositions in the present study were examined by SEM after chemically etching samples that had been isothermally crystallized at two temperatures: 90 °C and 130 °C (Fig. S9 jn the supporting information and Fig. 7, respectively). Conceptually, the poor solvent mixture dissolved the less crystalline and amorphous areas of the surface as well as the water-soluble PEG; only highly crystalline areas were left behind. At low T_c, SEM micrographs showed non-spherulitic, unordered structures similar to that of the low T_c PLA structures observed previously (supporting information Fig. S9) [29]. At low T_c, growth will be severely hindered and so a large amount of material remained amorphous/disordered and was dissolved during etching. Likewise, samples crystallized at low T_c exhibited smaller χ values upon reheating compared to high T_c, and crystallized structures, which were very small, would be expected to have low melting points like those observed (Fig. 5). High T_c conditions produced spherulites across all compositions. The centers, containing the nuclei of the spherulites, were also dissolved during etching. This has been observed by other authors for PLA and a potential reason for the etching out of centers is that the nuclei are disordered compared to the outer layers that are placed later [29,30]. This phenomenon was observed across all high T_c samples, but to different degrees along with spherulite size as nucleant type and concentration was varied.

The addition of PEG alone changed the crystal morphology of PLA. PLA spherulites were denser and fuller (very fine lamella), with distinct interfaces between neighboring spherulites comparable to those previously observed for high molecular weight PLA [29]. The addition of PEG produced large, coarse spherulites where small gaps between neighboring crystals could be observed; this space may be caused by the ejection or exclusion of PEG to the interface during crystallization. Additionally, larger pores or pockets of free space were observed in the samples after etching (Fig. 7C and D). The spherulites in Fig. 7 are not reminiscent of banded spherulites since they do not exhibit a periodic structure across the spherulite but are isolated. Two potential reasons are solute ejection and/or phase separation of the PEG during crystallization or spherulite fall-out/pull-out. Full phase separation is unlikely as no distinct melting or crystallization peaks around 15–25 °C, which correspond to low molecular weight PEG, were observed in the DSC thermograms (Fig. 4). However, solute ejection of the PEG ahead of the crystallization front may still be occurring if the PEG is simply higher in concentration and forming a solid solution. Studies on the solubility of PEG in PLA have reported that phase separation occurs above 10% and coincides with the appearance of a melting/crystallization peak in the

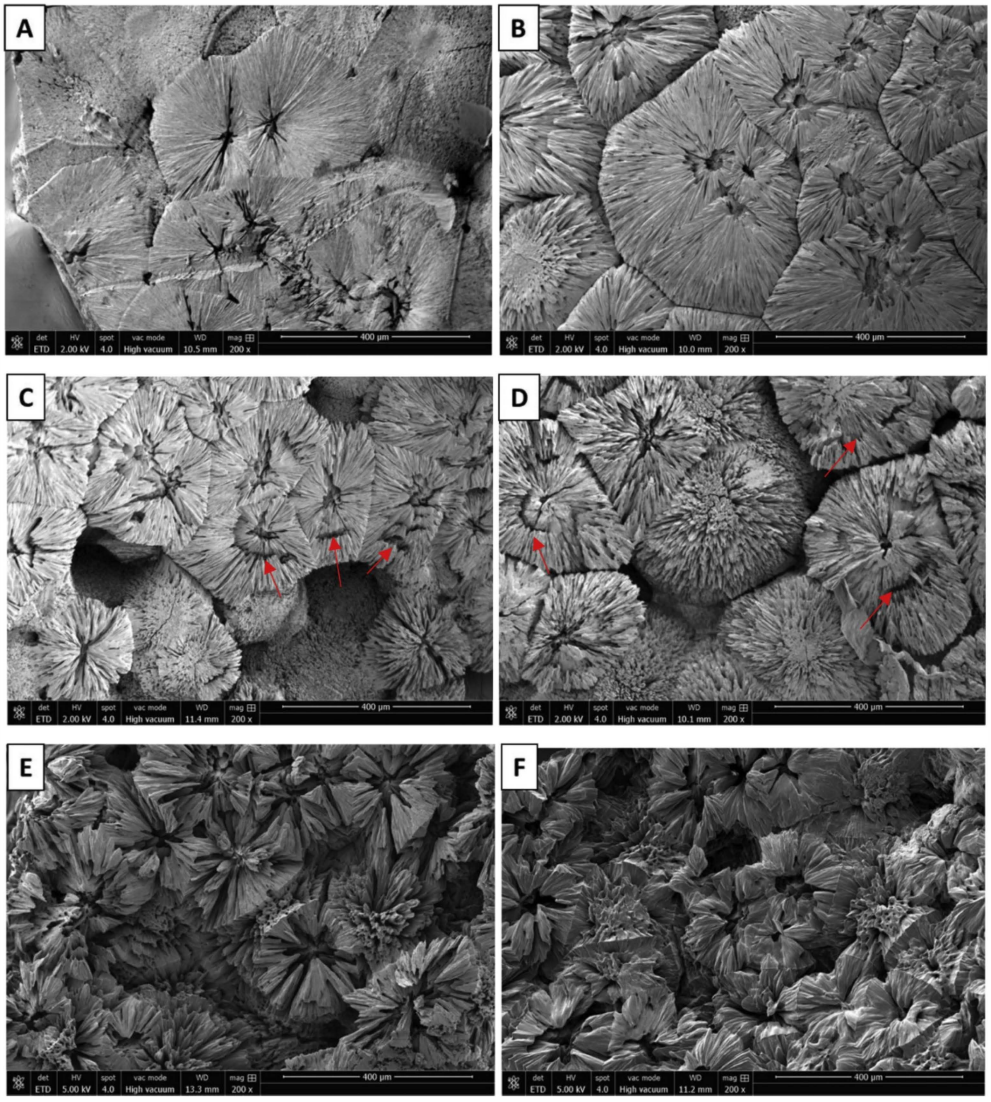

Fig. 7. Scanning electron micrographs of chemically etched specimens isothermally crystallized at 130 °C: A) Neat PLA, B) 5 wt% PEG, C) 0.05 wt% CNF-5 wt% PEG, D) 0.05 wt% CNC-5 wt%PEG, E) 0.55 wt% CNC-5 wt%PEG, and F) 0.05 wt% Talc-5 wt%PEG.

DSC thermogram [35], so that if solute ejection is happening, the concentration of PEG in PLA cannot be above this value. Thus, it is more likely that pull-out, where loose spherulites would have fallen out during chemical etching as the amorphous regions were dissolved, occurred instead, although any solute ejection that raises the PEG concentration locally at the periphery may make this more likely.

The addition of nucleation agents (CNC, CNF, or talc) resulted in additional changes to the crystal microstructure of PLA. Like the 5 wt% PEG, samples containing a nucleation agent and PEG also exhibited evidence of crystallite pull-out (Fig. 7C and D). Unlike the neat PLA, samples with additives are growing faster due to enhanced growth from mobility and nucleation and thus, significant coarsening of the microstructure is observed. Coarsening of the microstructure and large grain size can lead to poor mechanical performance. For the 0.05 wt% nanocellulose compositions, a shell microstructure can be observed around some crystallites (Fig. 7 C-D; Fig. 8). Although talc compositions did not exhibit a similar shell around spherulites, talc did show a slight reduction in size compared to samples containing nanocellulose or only PEG. As expected, talc is a good nucleation agent for PLA as many nuclei were formed, the crystallization rate was improved (Table 2) and the surface energy reduction (Table 3) was largest for talc.

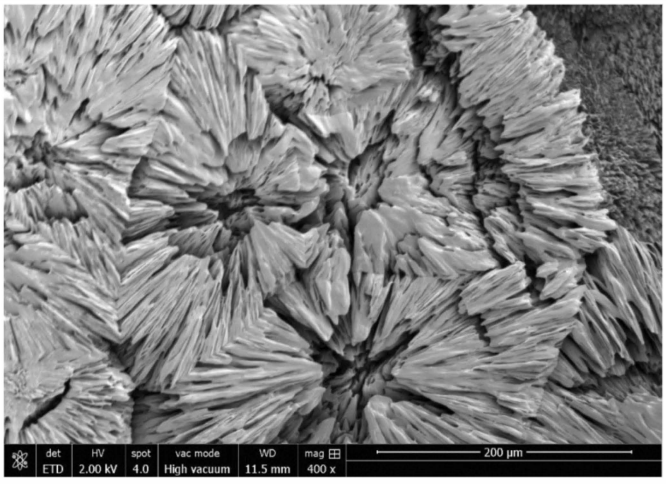

Fig. 8. Micrograph of 0.05% CNF-5%PEG isothermally crystallized at 130 °C and then chemically etched.

4. Conclusion

In the present study, polymer nanocomposites were prepared using PEG as a plasticizer and as a compatibilizer for CNC and CNF as nucleants for PLA, with talc being used as a commercial comparison. Very small concentrations of CNC and mechanically fibrillated CNF, similar to those used for commercial nucleation agents, were investigated as heterogenous nucleation agents using conventional kinetics approaches: Avrami and Lauritzen-Hoffman formalisms. Isothermal crystallization kinetics were studied for a wide temperature zone that spanned the temperature range where α' to α transitions. At high T_c, the CNC and CNF containing compositions were faster than talc. The Lauritzen-Hoffman analysis showed a decrease in the nucleation constant, K_g, and a decrease in the surface energy of folding, σ_e, suggesting that at very small concentrations CNC and CNF are good potential nucleation agents for PLA.

Additionally, the spherulite morphology was studied though chemical etching of the isothermally crystallized samples and morphologically, the nucleation agents produced very different results. For isothermal samples at $T_c = 130$ °C, the addition of 5 wt% PEG produced a coarse structure which was made coarser by the addition of CNC or CNF and suggested that these composites were indeed crystallizing faster at the higher T_c compared to talc. While the microscopy images cannot provide an estimate of spherulite size, the spherulites of the nanocellulose compositions did appear smaller, but not as small as the talc comparison group which exhibited both lower melting points in the DSC thermograms and visually smaller spherulites in the micrographs.

Overall, the CNC and CNF were found to be efficient nucleants with faster crystallization kinetics than talc, a commercial PLA nucleant, at high temperatures, and with a similar morphology for the concentrations examined. Importantly, CNF and, especially, CNC were found to give a significantly higher overall crystallinity, indicating that they may, ultimately, give better properties than the commonly used talc for the concentrations examined.

CRediT author statement

Caitlyn M. Clarkson- Conceptualization, methodology, formal analysis, investigation, writing- original draft.

Sami M. El Awad Azrak-Software, formal analysis, writing-review and editing.

Gregory T. Schueneman- Funding acquisition, writing-review and editing, supervision.

James F. Snyder- Funding acquisition, writing-review and editing, supervision.

Jeffrey P. Youngblood- Conceptualization, writing-review and editing, supervision.

https://www.elsevier.com/authors/journal-authors/policies-and-ethics/credit-author-statement.

Declaration of competing interest

The authors declare that they have no known competing financial interests or personal relationships that could have appeared to influence the work reported in this paper.

Acknowledgments

The authors would like to thank Professor Alejandro Müller for sharing the custom Origin Plugin used for the Avrami and Lauritzen-Hoffman analysis in this study.

The authors would like to acknowledge financial support from the Private-Public Partnership for Nanotechnology in the Forestry Sector (P3Nano) under Grant No. 107528, the Forest Products Laboratory Grant Number 17000384, and National Science Foundation Integrative Graduate Education and Research Traineeship: Sustainable Electronics Grant (Grant Number 1144843).

Appendix A. Supplementary data

Supplementary data to this article can be found online at https://doi.org/10.1016/j.polymer.2019.122101.

References

[1] D. Garlotta, A literature review of poly (lactic acid), J. Polym. Environ. 9 (2002) 63–84.
[2] R. Auras, B. Harte, S. Selke, An overview of polylactides as packaging materials, Macromol. Biosci. 4 (2004) 835–864, https://doi.org/10.1002/mabi.200400043.
[3] T.D. Ngo, A. Kashani, G. Imbalzano, K.T.Q. Nguyen, D. Hui, Additive manufacturing (3D printing): a review of materials , methods , applications and challenges, Compos. Part B. 143 (2018) 172–196, https://doi.org/10.1016/j.compositesb.2018.02.012.
[4] M. Jamshidian, E.A. Tehrany, M. Imran, M. Jacquot, S. Desobry, Poly-Lactic Acid: production, applications, nanocomposites, and release studies, Compr. Rev. Food Sci. Food Saf. 9 (2010) 552–571, https://doi.org/10.1111/j.1541-4337.2010.00126.x.
[5] R.J. Moon, A. Martini, J. Nairn, J. Simonsen, J. Youngblood, Cellulose nanomaterials review: structure, properties and nanocomposites, Chem. Soc. Rev. 40 (2011) 3941–3994, https://doi.org/10.1039/c0cs00108b.
[6] Y. Habibi, Key advances in the chemical modification of nanocelluloses, Chem. Soc. Rev. 43 (2014) 1519–1542, https://doi.org/10.1039/C3CS60204D.
[7] Y. Habibi, S. Aouadi, J.M. Raquez, P. Dubois, Effects of interfacial stereocomplexation in cellulose nanocrystal-filled polylactide nanocomposites, Cellulose 20 (2013) 2877–2885, https://doi.org/10.1007/s10570-013-0058-5.
[8] J.A. Diaz, Z. Ye, X. Wu, A.L. Moore, R.J. Moon, A. Martini, D.J. Boday, J. P. Youngblood, Thermal conductivity in nanostructured films: from single cellulose nanocrystals to bulk films, Biomacromolecules 15 (2014) 4096–4101, https://doi.org/10.1021/bm501131a.
[9] J.A. Diaz, X. Wu, A. Martini, J.P. Youngblood, R.J. Moon, Thermal expansion of self-organized and shear-oriented cellulose nanocrystal films, Biomacromolecules 14 (2013) 2900–2908, https://doi.org/10.1021/bm400794e.
[10] R.A. Chowdhury, M. Nuruddin, C. Clarkson, F. Montes, J. Howarter, P. J. Youngblood, Cellulose nanocrystal (CNCe) coatings with controlled anisotropy as high-performance gas barrier films, ACS Appl. Mater. Interfaces (2019) 1376–1383, https://doi.org/10.1021/acsami.8b16897.
[11] S.X. Peng, H. Chang, S. Kumar, R.J. Moon, J.P. Youngblood, A comparative guide to controlled hydrophobization of cellulose nanocrystals via surface esterification, Cellulose 23 (2016) 1825–1846, https://doi.org/10.1007/s10570-016-0912-3.
[12] Y. Yoo, J.P. Youngblood, Green one-pot synthesis of surface hydrophobized cellulose nanocrystals in aqueous medium, ACS Sustain. Chem. Eng. 4 (2016) 3927–3938, https://doi.org/10.1021/acssuschemeng.6b00781.
[13] O. Martin, L. Avérous, Poly(lactic acid): plasticization and properties of biodegradable multiphase systems, Polymer 42 (2001) 6209–6219, https://doi.org/10.1016/S0032-3861(01)00086-6.
[14] H. Li, M.A. Huneault, Effect of nucleation and plasticization on the crystallization of poly(lactic acid), Polymer 48 (2007) 6855–6866, https://doi.org/10.1016/j.polymer.2007.09.020.
[15] M.A. Huneault, H. Li, Morphology and properties of compatibilized polylactide/thermoplastic starch blends, Polymer 48 (2007) 270–280, https://doi.org/10.1016/j.polymer.2006.11.023.
[16] M.J. Sobkowicz, J.R. Dorgan, K.W. Gneshin, A.M. Herring, J.T. McKinnon, Renewable cellulose derived carbon nanospheres as nucleating agents for polylactide and polypropylene, J. Polym. Environ. 16 (2008) 131–140, https://doi.org/10.1007/s10924-008-0093-8.
[17] M. Vestena, I.P. Gross, C.M.O. Muller, A.T.N. Pires, Nanocomposite of poly(lactic acid)/cellulose nanocrystals: effect of CNC content on the polymer crystallization kinetics, J. Braz. Chem. Soc. 27 (2016) 905–911.
[18] A. Gupta, W. Simmons, G.T. Schueneman, E.A. Mintz, Lignin-coated cellulose nanocrystals as promising nucleating agent for poly(lactic acid), J. Therm. Anal. Calorim. 126 (2016) 1243–1251, https://doi.org/10.1007/s10973-016-5657-6.
[19] C.M. Clarkson, G. Schueneman, J. Synder, J.P. Youngblood, Dry-spinning of cellulose nanocrystal/polylactic acid composite fibers, Green Mater. 6 (2018) 1–9, https://doi.org/10.1680/jgrma.17.00027.
[20] N. Herrera, A.P. Mathew, K. Oksman, Plasticized polylactic acid/cellulose nanocomposites prepared using melt-extrusion and liquid feeding: mechanical, thermal and optical properties, Compos. Sci. Technol. 106 (2015) 149–155, https://doi.org/10.1016/j.compscitech.2014.11.012.
[21] Y. Lu, M.C. Cueva, E. Lara-Curzio, S. Ozcan, Improved mechanical properties of polylactide nanocomposites-reinforced with cellulose nanofibrils through interfacial engineering via amine-functionalization, Carbohydr. Polym. 131 (2015) 208–217, https://doi.org/10.1016/j.carbpol.2015.05.047.
[22] C.M. Clarkson, S.M. El Awad Azrak, R. Chowdhury, S.N. Shuvo, J. Snyder, G. Schueneman, V. Ortalan, J.P. Youngblood, Melt spinning of cellulose nanofibril/polylactic acid (CNF/PLA) composite fibers for high stiffness, ACS Appl. Polym. Mater. 1 (2019) 166–168, https://doi.org/10.1021/acsapm.8b00030.
[23] H. Wu, S. Nagarajan, L. Zhou, Y. Duan, J. Zhang, Synthesis and characterization of cellulose nanocrystal-graft-poly(D-lactide) and its nanocomposite with poly(L-

lactide), Polymer 103 (2016) 365–375, https://doi.org/10.1016/j.polymer.2016.09.070.
[24] S. Fujisawa, J. Zhang, T. Saito, T. Iwata, A. Isogai, Cellulose nanofibrils as templates for the design of poly(l-lactide)- nucleating surfaces, Polymer 55 (2014) 2937–2942, https://doi.org/10.1016/j.polymer.2014.04.019.
[25] S. Fujisawa, T. Saito, S. Kimura, T. Iwata, A. Isogai, Surface engineering of ultrafine cellulose nanofibrils toward polymer nanocomposite materials, Biomacromolecules 14 (2013) 1541–1546, https://doi.org/10.1021/bm400178m.
[26] M.J. John, R. Anandjiwala, K. Oksman, A.P. Mathew, Melt-spun polylactic acid fibers: effect of cellulose nanowhiskers on processing and properties, J. Appl. Polym. Sci. 127 (2013) 274–281, https://doi.org/10.1002/app.37884.
[27] A.P. Mathew, K. Oksman, M. Sain, The effect of morphology and chemical characteristics of cellulose reinforcements on the crystallinity of polylactic acid, J. Appl. Polym. Sci. 101 (2006) 300–310, https://doi.org/10.1002/app.23346.
[28] E.M. Sullivan, R.J. Moon, K. Kalaitzidou, Processing and characterization of cellulose nanocrystals/polylactic acid nanocomposite films, Materials 8 (2015) 8106–8116, https://doi.org/10.3390/ma8125447.
[29] Y. He, Z. Fan, Y. Hu, T. Wu, J. Wei, S. Li, DSC analysis of isothermal melt-crystallization , glass transition and melting behavior of poly (L -lactide) with different molecular weights, Polymer 43 (2007) 4431–4439, https://doi.org/10.1016/j.eurpolymj.2007.07.007.
[30] B.E.W. Fischer, H.J. Sterzel, G. Wegner, Investigation of the structure of solution grown crystals of lacride copolymers by means of chemical reactions, Polymere 990 (1973) 980–990.
[31] P. Pan, Y. Inoue, Polymorphism and isomorphism in biodegradable polyesters, Prog. Polym. Sci. 34 (2009) 605–640, https://doi.org/10.1016/j.progpolymsci.2009.01.003.
[32] J. Zhang, H. Tsuji, I. Noda, Y. Ozaki, Structural changes and crystallization dynamics of poly(L-lactide) during the cold-crystallization process investigated by infrared and two-dimensional infrared correlation spectroscopy, Macromolecules 37 (2004) 6433–6439, https://doi.org/10.1021/ma049288t.
[33] J. Zhang, K. Tashiro, H. Tsuji, A.J. Domb, Disorder-to-order phase transition and multiple melting behavior of poly(L-lactide) investigated by simultaneous measurements of WAXD and DSC, Macromolecules 41 (2008) 1352–1357, https://doi.org/10.1021/ma0706071e
[34] B.W. Chieng, N.A. Ibrahim, W.M.Z.W. Yunus, M.Z. Hussein, Plasticized poly(lactic acid) with low molecular weight poly(ethylene glycol): mechanical, thermal, and morphology properties, J. Appl. Polym. Sci. 130 (2013) 4576–4580, https://doi.org/10.1002/app.39742.
[35] K. Sungsanit, N. Kao, S.N. Bhattacharya, Properties of linear poly(lactic acid)/polyethylene glycol blends, Polym. Eng. Sci. 52 (2012) 108–116, https://doi.org/10.1002/pen.22052.
[36] X. Meng, V. Bocharova, H. Tekinalp, S. Cheng, A. Kisliuk, A.P. Sokolov, V. Kunc, W. H. Peter, S. Ozcan, Toughening of nanocelluose/PLA composites via bio-epoxy interaction: mechanistic study, Mater. Des. 139 (2018) 188–197, https://doi.org/10.1016/j.matdes.2017.11d012.
[37] A.T. Lorenzo, M.L. Arnal, J. Albuerne, A.J. Müller, DSC isothermal polymer crystallization kinetics measurements and the use of the Avrami equation to fit the data: guidelines to avoid common problems, Polym. Test. 26 (2007) 222–231, https://doi.org/10.1016/j.polymertesting.2006.10.005.
[38] J.M. Schultz, Polymer Crystallization: the Development of Crystalline Order in Thermoplastic Polymers, Oxford University Press, Inc., New York, 2001.
[39] S. Iannace, L. Nicolais, Isothermal crystallization and chain mobility of of poly (L -lactide), J. Appl. Polym. Sci. 64 (1997) 911–919.
[40] Y. Li, C. Han, Y. Yu, L. Xiao, Y. Shao, Crystallization behaviors of poly (lactic acid) composites fabricated using functionalized eggshell powder and poly (ethylene glycole), Thermochim. Acta 663 (2018) 67–76, https://doi.org/10.1016/j.tca.2018.03.011e
[41] I. Pillin, N. Montrelay, Y. Grohens, Thermo-mechanical characterization of plasticized PLA : is the miscibility the only significant factor ? Polymer 47 (2006) 4676–4682, https://doi.org/10.1016/j.polymer.2006.04.013.
[42] H. Li, M.A. Huneault, Effect of nucleation and plasticization on the crystallization of poly (lactic acide), Polymer 48 (2007) 6855–6866, https://doi.org/10.1016/j.polymer.2007.09.020.
[43] V. Khoshkava, M.R. Kamal, Effect of surface energy on dispersion and mechanical properties of polymer/nanocrystalline cellulose nanocomposites, Biomacromolecules 14 (2013) 3155–3163, https://doi.org/10.1021/bm400784j.
[44] S. Chen, G. Schueneman, R.B. Pipes, J. Youngblood, R.J. Moon, Effects of crystal orientation on cellulose nanocrystals – cellulose acetate nanocomposite fibers prepared by dry spinning, Biomacromolecules 15 (2014) 3827–3835, https://doi.org/10.1021/bm501161v.
[45] S. Beck, J. Bouchard, R. Berry, Dispersibility in water of dried nanocrystalline cellulose, Biomacromolecules 13 (2012) 1486–1494, https://doi.org/10.1021/bm300191k.
[46] M.N. Angles, A. Dufresne, Plasticized starch/tunicin whiskers nanocomposites. 1. Structural analysis, Macromolecules 33 (2000) 8344–8353, https://doi.org/10.1021/ma0008701.
[47] J.C. Liu, D.J. Martin, R.J. Moon, J.P. Youngblood, Enhanced thermal stability of biomedical thermoplastic polyurethane with the addition of cellulose nanocrystals, J. Appl. Polym. Sci. 132 (2015) 1–8, https://doi.org/10.1002/app.41970.
[48] M.S. Reid, H.S. Marway, C. Moran-Hidalgo, M. Villalobos, E.D. Cranston, Comparison of polyethylene glycol adsorption to nanocellulose versus fumed silica in water, Cellulose 24 (2017) 4743–4757, https://doi.org/10.1007/s10570-017-1482-8.
[49] T. Kawai, N. Rahman, G. Matsuba, K. Nishida, T. Kanaya, M. Nakano, H. Okamoto, J. Kawada, A. Usuki, N. Honma, K. Nakajima, M. Matsuda, Crystallization and melting behavior of poly (L-lactic acid), Macromolecules 40 (2007) 9463–9469, https://doi.org/10.1021/ma070082c.
[50] H.W. Xiao, P. Li, X. Ren, T. Jiang, J. Yeh, Isothermal crystallization kinetics and crystal structure of poly (lactic acid): effect of triphenyl phosphate and talc, J. Appl. Polym. Sci. 118 (2010) 3558–3569, https://doi.org/10.1002/app.
[51] H. Tsuji, H. Takai, S.K. Saha, Isothermal and non-isothermal crystallization behavior of poly(l-lactic acid): effects of stereocomplex as nucleating agent, Polymer 47 (2006) 3826–3837, https://doi.org/10.1016/j.polymer.2006.03.074.
[52] H. Tsuji, Y. Ikada, Properties and morphologies of poly(L-lactide): 1. Annealing condition effects on properties and morphologies of poly(L-lactide), Polymer 36 (1995) 2709–2716.
[53] P. Pan, W. Kai, B. Zhu, T. Dong, Y. Inoue, Polymorphous crystallization and multiple melting behavior of poly (L -lactide): molecular weight dependence, Macromolecules 40 (2007) 6898–6905, https://doi.org/10.1021/ma071258d.
[54] H. Marand, J. Xu, S. Srinivas, Determination of the equilibrium melting temperature of polymer Crystals : linear and nonlinear Hoffman - weeks extrapolations, Macromolecules 31 (1998) 8219–8229, https://doi.org/10.1021/ma980747y.
[55] G.Z. Papageorgiou, D.S. Achilias, S. Nanaki, T. Beslikas, D. Bikiaris, PLA nanocomposites : effect of filler type on non-isothermal crystallization, Thermochim. Acta 511 (2010) 129–139, https://doi.org/10.1016/j.tca.2010.08.004.
[56] G. Sun, L.T. Weng, J.M. Schultz, C.M. Chan, Formation of banded and non-banded poly(l-lactic acid) spherulites during crystallization of films of poly(l-lactic acid)/poly(ethylene oxide) blends, Polymer 55 (2014) 1829–1836, https://doi.org/10.1016/j.polymer.2014.02.036.
[57] S. Nurkhamidah, E.M. Woo, Effects of stereocomplex nuclei or spherulites on crystalline morphology and crack behavior of poly(L -lactic acid), Macromol. Chem. Phys. 212 (2011) 1663–1670, https://doi.org/10.1002/macp.201100207.
[58] S. Nurkhamidah, E.M. Woo, Effects of crystallinity and molecular weight on crack behavior in crystalline poly(L-lactic acid), J. Appl. Polym. Sci. 122 (2011) 1976–1985, https://doi.org/10.1002/app.